

## Structural defects and electrochemical reactivity of $\beta$ -Ni(OH)<sub>2</sub>

M.C. Bernard <sup>a,\*</sup>, R. Cortes <sup>a</sup>, M. Keddad <sup>a</sup>, H. Takenouti <sup>a</sup>, P. Bernard <sup>b</sup>, S. Senyari <sup>b</sup>

<sup>a</sup> UPR 15 CNRS, Physique des Liquides et Electrochimie, Université P. et M. Curie, CP 133, 4 place Jussieu, 75 252 Paris Cedex 05, France

<sup>b</sup> SAFT, Direction de la Recherche, route de Nozay, 91 460 Marcoussis, France

Received 4 April 1996; revised 9 September 1996; accepted 30 September 1996

### Abstract

Electrochemical reactivities and structural properties of several nickel hydroxide powders were analysed by X-ray diffraction, Raman spectroscopy and extended X-ray absorption fine structure (EXAFS). It is shown that the electrochemical efficiency of  $\beta$ -Ni(OH)<sub>2</sub> is associated with the amount of proton vacancies included in the crystal lattice. The number of those proton vacancies increases when the crystallite size decreases or when the ratio of co-precipitated cobalt increases. Proton vacancies shift the oxidation potential of  $\beta$ -Ni(OH)<sub>2</sub> towards less anodic values and, therefore, improve the chargeability and the electrochemical efficiency of nickel hydroxide. It is shown that both Raman spectroscopy and X-ray diffraction techniques can be used to predict effectively the electrochemical efficiency of  $\beta$ -Ni(OH)<sub>2</sub> hydroxide. EXAFS results indicate also that the oxidation level of nickel atoms inside the hydroxide is not modified by the existence of proton vacancies. It means probably that to maintain the electroneutrality in the whole crystal induces others singularities. Finally, the influence of co-precipitated additives such as cadmium and cobalt on the rate of defects has been investigated.

**Keywords:** Nickel hydroxide; Alkaline batteries; Structural defects; Electrochemical reactivity

### 1. Introduction

The nickel hydroxide/nickel oxyhydroxide couple is the main redox system used in the positive electrode of alkaline rechargeable batteries, because its reversibility and cyclic behaviour are good. To increase the specific capacity (a maximum charge stored in a given volume of electrode) of the active material, a new technology based on a 'foam' electrode was recently introduced [1–4]. The active material, nickel hydroxide particles, is pasted into a highly porous metallic nickel matrix, which works as an electrical collector (connection between the hydroxide particles and the external circuit).

In the present work, five types of  $\beta$ -Ni(OH)<sub>2</sub> powder samples with different physical characteristics were chemically prepared and then introduced into a nickel foam substrate, and used as the positive hydroxide nickel electrode in Ni–Cd rechargeable batteries. Their electrochemical properties were evaluated and compared with their structural characteristics observed from X-ray diffraction, Raman spectroscopy, and extended X-ray absorption fine structure (EXAFS) studies to make a relation between the structural parameters and the electrochemical reactivity of  $\beta$ -Ni(OH)<sub>2</sub>.

### 2. Experimental

#### 2.1. Preparation of nickel electrode

Five nickel hydroxides (marked A to E) were chemically prepared, using a synthesis method described in Ref. [5] by modifying the temperature and the reaction time. The five nickel hydroxides were then used as the materials for positive electrodes, prepared as follows. Nickel hydroxide powder and cobalt hydroxide powder were mixed at a weight ratio of 92:8, and an aqueous suspension containing 0.5 wt.% of carboxymethyl cellulose (CMC) was added to the mixture in order to obtain a paste. This paste was filled in a nickel porous foam (Nitech), dried at 90 °C for 1 h, pressed and cut into 9.5 cm × 5 cm to obtain a nickel hydroxide positive electrode. An Ni–Cd flooded cell was then assembled with the positive electrode, two negative sintered electrodes and a polyamide separator. 50 cm<sup>3</sup> of an alkaline electrolyte composed of 9.1 N potassium hydroxide solution and 0.2 N lithium hydroxide solution was poured therein. The rechargeable cells were placed in a thermoregulated room at 20 °C (±2 °C) and charged initially at 0.1C<sub>10</sub> rate for 10 h. C<sub>10</sub> corresponds to the current needed to discharge the total capacity of the positive electrode in 1 h. The cells were discharged at 0.2C<sub>10</sub> rate down to 1 V. Afterwards, the cells were cycled according to the following conditions until their discharge capacity was stable:

\* Corresponding author.

charge at 0.2Cn rate for 7.5 h, discharge at the same rate down to 1 V.

## 2.2. Physical and chemical analysis of nickel hydroxide samples

The chemical composition of the five nickel hydroxide samples (A to E) was measured with an atomic absorption spectrometer Varian AA875. Samples A–E were cobalt and cadmium nickel hydroxide added type, containing 1 wt.% of  $\text{Co}(\text{OH})_2$  ( $\pm 0.2\%$ ) and 9 wt.% of  $\text{Cd}(\text{OH})_2$  ( $\pm 0.5\%$ ).

X-ray diffraction (XRD) analysis were carried out using a Siemens D5000XR diffractometer equipped with a graphite monochromator and Cu  $K\alpha$  radiation. The spectra were registered at  $0.015^\circ/\text{s}$ .

The nickel hydroxide powders were studied by Micro-Raman spectroscopy using a Dilor multichannel spectrometer with a 514.5 nm line of an argon laser. The beam was focused to a spot size of about  $1\ \mu\text{m}$  and the output power at the laser was set to 50 mW. The integration time for spectrum collection with a Dilor multichannel detector was set to 2 s.

EXAFS studies were performed at the liquid helium temperature at LURE-DCI (Orsay) using the XAS II spectrometer with Si (311) monochromator. During the measurements, the synchrotron was operating typically at an energy of 1.85 GeV, with an average beam current of 300 mA. The results were collected over an energy range of 1000 eV by steps of 2 eV. The Ni  $k$ -edge is approximately 8333 eV. EXAFS signals were recorded by measuring  $I_0(E)$  and  $I_1(E)$  for each energy value, with two ionisation chambers. Intensity measurements are very sensitive to the quality of the samples, great care is therefore needed for their preparation. In particular, their thickness must be as constant as possible. Each hydroxide was ground to obtain  $1\ \mu\text{m}$  particles, and 14 mg of this powder was mixed with 10 mg of cellulose. The powder mixture was then pressed into a pellet, whose apparent surface area was  $2\ \text{cm}^2$ .

## 3. Results

### 3.1. Electrochemical measurements

The five nickel hydroxides discharge capacities were measured after stabilisation of the electrochemical efficiency. As shown in Table 1, the discharge capacities decreased from sample A to sample E. The first charging curve for sample A and sample E is shown in Fig. 1. The charging potential of

Table 1  
Battery capacity of  $\text{Ni}(\text{OH})_2$  of different crystallite size

Hydroxide	A	B	C	D	E
Efficiency at C/5 rate discharge ( $\text{mAh g}^{-1}$ )	270	251	221	207	180

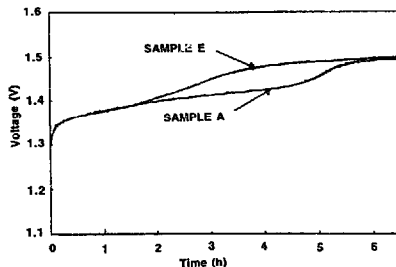


Fig. 1. Charging curves at C/5 rate during the first oxidation of the hydroxides A and E.

sample A is lower than that of sample E, on which oxygen evolution takes place precociously. The electrical curves of the other  $\text{Ni}(\text{OH})_2$  samples are not given, but the charging potential at half-charge decreases from sample E to sample A.

After the electrochemical evaluation of the five nickel hydroxide, the structure of these compounds was analysed; these studies reported in the following sections were carried out exclusively on uncycled nickel hydroxide particles.

### 3.2. XRD patterns

The structure of the five nickel hydroxides was examined by XRD and the results are shown in Fig. 2. All hydroxides exhibit XRD characteristics of the  $\beta$ - $\text{Ni}(\text{OH})_2$  phase, but the width of several peaks indicates that their degree of crystallinity is different. It is found that the broader the XRD peak, the greater is the charge capacity (for a given amount of hydroxide). This fact has already been observed [6,9]. Terasaka et al. [7] have linked the electrochemical efficiency to the width of the (101) peak, and Watanabe et al. [8] to that of both the (001) and the (101) peaks. This work shows that other peaks are modified when the hydroxide is more reactive, and some (namely 101, 102, 103) are particularly relevant to the electrochemical reactivity, as shown in Fig. 3 and Table 2.

The crystallite size is usually evaluated from the width of the diffraction peaks according to Scherrer's formula [10]. Also, the sizes calculated from the (001) and (100) peaks can be compared with those measured from the transmission electron microscopy (TEM) picture of hydroxide A (Fig. 4). In this figure, we notice that the crystallites are pellet-like, observed on the edge, and their dimensions are close to those calculated from the width of XRD peaks ( $100\ \text{\AA}$  in width and  $400\ \text{\AA}$  in length). A good agreement between the observed and the calculated dimensions has also been found for the other hydroxides. Nevertheless, such an agreement is not obtained crosswise. For example, the size in the direction perpendicular to the [101] plane, calculated from the width of the (101) peak is much smaller than that calculated by a geometrical way using the crystallite size observed by TEM.

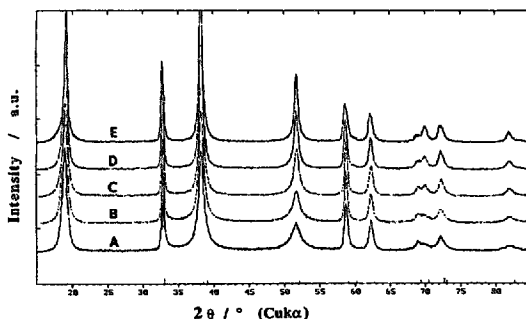
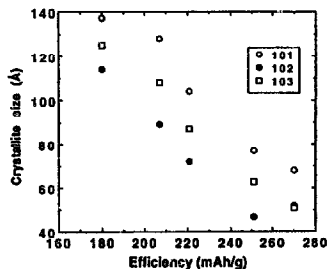


Fig. 2. XRD patterns of the nickel hydroxides A-E, see Table 1.

Table 2

Crystallite sizes calculated from the width of the X-ray diffraction peaks

Sample	C.S. 001 (Å)	C.S. 100 (Å)	C.S. 101 (Å)	C.S. 102 (Å)	C.S. 110 (Å)	C.S. 111 (Å)	C.S. 103 (Å)	C.S. 201 (Å)	C.S. 202 (Å)	<i>l</i> (Å)
A	85	195	68	52	157	123	51	80	52	148
B	84	219	77	47	180	134	63	97	49	159
C	76	250	104	72	192	132	87	111	78	168
D	106	244	128	89	176	146	108	112	76	185
E	126	242	137	114	130	131	125	105	96	195

Fig. 3. Electrochemical efficiency of  $\beta$ -Ni(OH)<sub>2</sub>, as a function of the crystallite size evaluated in some specific directions.

Such a result suggests the existence of defects in the whole volume of the material because the length of coherence of the crystal is crosswise smaller than its physical size. An average length, taking into account the whole volume of the hexagonal lattice may also be evaluated using the following formula

$$l = (A^2C)^{1/3} \quad (1)$$

where  $A$  is the crystallite size in the direction perpendicular to the [100] plane, and  $C$  the crystallite size in the direction perpendicular to the [001] plane.

One may observe that this calculated length (called  $l$ ), as the different lengths evaluated from all the diffraction peaks relative to crosswise directions (i.e. (101), (102), (103), (202)) can be correlated with the efficiency of the nickel hydroxide is presented in Table 2.

Some structural defects are distributed among the volume of the crystal lattice; the bigger the amount of defects, the more efficient the hydroxide.

The study of the XRD patterns indicate also that the  $a$  and  $c$  crystallographic parameters of the hexagonal unit lattice of  $\beta$ -Ni(OH)<sub>2</sub> are quite different from sample A to sample E, see Table 3. In particular, the  $a$  and  $c$  parameters become closer to those of  $\beta$ -NiOOH when the efficiency of the hydroxide increases.

It is well known that from  $\beta$ -Ni(OH)<sub>2</sub> to  $\beta$ -NiOOH, the  $a$  lattice parameter becomes lower because of the decrease of the ionic radius of the nickel atoms, and the  $c$  lattice parameter becomes greater because the electrostatic charge repulsion between the Ni(OH)<sub>2</sub> slabs increases.

Some structural characteristics of  $\beta$ -NiOOH may be present in a weak proportion in a badly crystallised Ni(OH)<sub>2</sub>. More particularly, the existence of proton vacancies located in the bulk of the crystalline lattice could be suggested.

### 3.3. Raman spectroscopy experiments

Raman spectroscopy experiments were carried out to understand the reason why some  $\beta$ -Ni(OH)<sub>2</sub> are more reac-

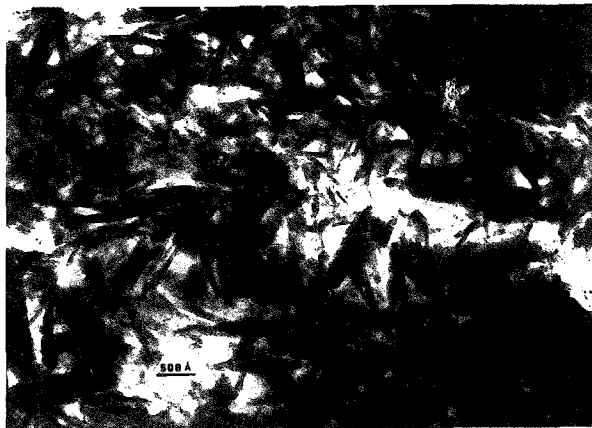


Fig. 4. TEM micrography of hydroxide A.

tive than others, and if the crystallite size is the only parameter determining their electrochemical efficiency.

The Raman spectrum of the well-crystallized  $\beta$ -Ni(OH)<sub>2</sub> is characterised by three Raman peaks at respectively 3570, 445 and 310 cm<sup>-1</sup>. A fourth peak at 380 cm<sup>-1</sup> has been also detected, but its intensity is very weak. The 3570 cm<sup>-1</sup> peak is attributed to the symmetric stretching of the hydroxyl groups ( $\nu$ OH) where only the hydrogen atom actually vibrates [11]. The position of this peak indicates that the hydroxyl groups are not hydrogen bonded. The band at 445 cm<sup>-1</sup> is assigned to the Ni-O stretching ( $\nu$ NiO) as corroborated by deuterium experiments [12], and the signal at 310 cm<sup>-1</sup> has been attributed to an E-type vibration of the Ni-OH lattice.

In comparison with the well-crystallised  $\beta$ -Ni(OH)<sub>2</sub>, the Raman spectra of compounds A to E displayed three additional peaks, in agreement with the spectrum obtained by Cornilsen et al. [13] for disordered  $\beta$ -Ni(OH)<sub>2</sub>, at respectively 3680, 3580 and 510 cm<sup>-1</sup> as shown in Fig. 5. Those peaks have never been attributed to particular vibration modes yet, but it is probable that both of them are associated with OH stretching of free hydroxyl groups (peaks at 3680 and 3580 cm<sup>-1</sup>). It is worthwhile to notice that the surface of the three additional peaks increased as the degree of crystallinity of the nickel hydroxide decreased, when their electrochemical reactivity was greater. Since the compounds A to E examined in this study do not correspond to a well-crystallised hydroxide, they will be called badly crystallised nickel hydroxide or  $\beta_{bc}$ -Ni(OH)<sub>2</sub> instead of  $\beta$ -Ni(OH)<sub>2</sub>, as proposed by Faure et al. [14].

The fundamental question to be considered is whether those three peaks are merely related to the Ni(OH)<sub>2</sub> crystallite size. A smaller crystallite size may imply a larger extended surface area of crystallites for a given amount of

material. Those peaks can also be due to the modification of some chemical bonds, caused by some structural defects. The concept of defects in nickel hydroxide has already been introduced in Refs. [15,16]. These defects may correspond to a partial break-down of the structure symmetry, leading to the appearance of new Raman peaks. Two A and E hydroxides showing the greatest and the smallest charge capacity were immersed in water in order to determine whether the three additional peaks are merely related to the surface area or due to structural defects in the bulk of the active material. Then their Raman spectrum were recorded. It is expected that the addition of water will hinder markedly the stretching of the free OH groups located at the surface of the crystallites which are likely to be combined with water molecules (hydrogen bonds).

### 3.3.1. OH stretching

As shown in Fig. 6, the 3680 cm<sup>-1</sup> peak disappeared completely indicating that it is associated with the stretching of the free OH<sup>-</sup> groups of the outer part of the crystallites. Those OH<sup>-</sup> groups, located at the crystallite surface, vibrate more easily than the OH<sup>-</sup> groups in the crystallite bulk, whose oscillations are characterised by the most intense peak at 3570 cm<sup>-1</sup>. This latter was not modified by the addition of water.

The 3580 cm<sup>-1</sup> shoulder was not modified either, suggesting that it is linked with OH<sup>-</sup> groups of the bulk. However, those groups do not vibrate exactly at the same frequency as those of the other bulk hydroxyl groups. However, only 10 cm<sup>-1</sup> separate their respective peaks indicating that their environment is only slightly different. The 3580 cm<sup>-1</sup> shoulder could therefore be likely due to the second layer of OH<sup>-</sup>, the first one being that of the external hydroxyl groups. This hypothesis is based on the fact that the surface

Table 3  
Crystallographic parameters of different  $\beta\text{-Ni}(\text{OH})_2$ 's

Hydroxide	$\beta\text{-NiOOH}$	A	B	C	D	E	$\beta\text{-Ni}(\text{OH})_2$
$a$ (Å)	2.81	3.142	3.146	3.144	3.146	3.150	3.12
$c$ (Å)	4.84	4.683	4.646	4.641	4.636	4.629	4.60

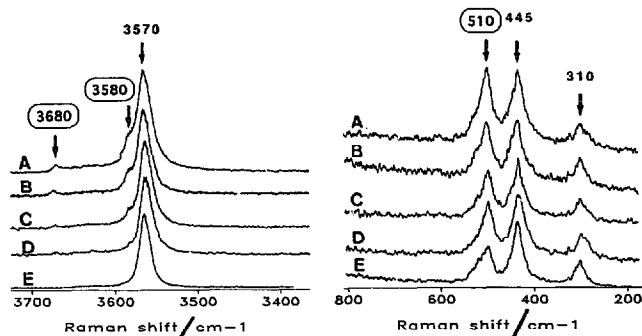


Fig. 5. Raman spectra of the nickel hydroxides A-E, see Table 1.

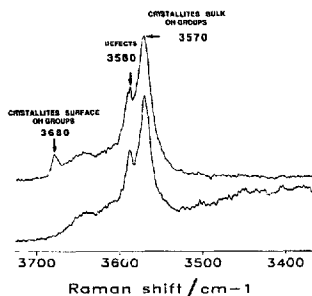


Fig. 6. Effect of the addition of water on the  $\text{OH}^-$  stretching zone ( $\nu_{\text{OH}}$ ).

of  $3580\text{ cm}^{-1}$  peak is always similar to that of the  $3680\text{ cm}^{-1}$  peak, for each  $\beta\text{-Ni}(\text{OH})_2$  studied here.

### 3.3.2. The peak at $510\text{ cm}^{-1}$

When water was added, the intensity of this peak decreased but did not disappear completely. This suggests that the  $510\text{ cm}^{-1}$  peak can be associated with the existence of defects. The fact that the peak never vanished supports the existence of both bulk and surface defects. The decrease of this peak intensity is therefore associated with defects located at the crystallite surface. Conversely, the remaining peak (after the addition of water) is probably due to bulk defects. The existence of surface defects is corroborated by the fact that the intensity decrease is more marked in the case of the compound A, having the greatest surface area, Fig. 7(a) and (b). More-

over, after water addition, the  $510\text{ cm}^{-1}$  peak intensity remained greater for compound A than that of compound E, Fig. 8. This may indicate that the number of bulk defects is greater when the hydroxide is poorly crystallised since the stretching surface defects were hindered by water molecules.

The Raman spectroscopy experiments show that both the  $3680$  and the  $3580\text{ cm}^{-1}$  peak intensities are proportional to the surface area of the crystallites constituting nickel hydroxide, because those peaks are due to  $\text{OH}^-$  ions located at or near this surface. On the contrary, the  $510\text{ cm}^{-1}$  peak is associated with structural defects. The nature of these defects will be discussed below. According to this interpretation, the origin of the three supplementary Raman peaks is given in Fig. 9.

### 3.3.3. Suggestions about the nature of defects

The origin of the  $510\text{ cm}^{-1}$  peak may be discussed in analogy with that of  $550\text{ cm}^{-1}$  peak exhibited by the oxyhydroxide nickel  $\beta\text{-NiOOH}$ . The fundamental difference between  $\beta\text{-Ni}(\text{OH})_2$  and  $\beta\text{-NiOOH}$  is the  $\text{H}_2\text{O}$  ratio. Assuming that both the  $510$  and  $550\text{ cm}^{-1}$  peaks are associated with  $\text{Ni-O}$  vibration when the oxygen atom is not linked with a proton, the defects related with these peaks may then be attributed to proton vacancies. In other words, if the major  $\text{Ni}^{2+}$  species were associated with  $\text{OH}^-$  groups, some of them might be located at the vicinity of  $\text{O}^{2-}$  (proton vacancy). Unfortunately, this explanation does not satisfy the principle of electro-neutrality. Proton vacancies induce an excess of negative charges which should be compensated for. EXAFS experiments have been carried out in order to better characterise the nature of the defects.

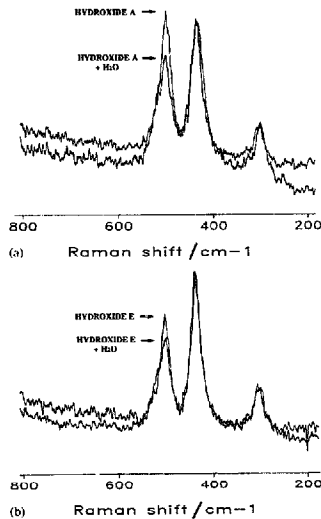


Fig. 7. Effect of the addition of water on the  $510\text{ cm}^{-1}$  peak: (a) hydroxide A, and (b) hydroxide E.

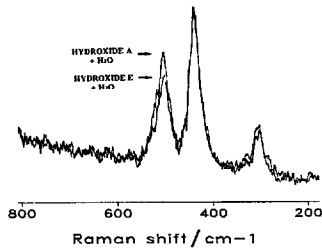


Fig. 8. Remaining intensity of the  $510\text{ cm}^{-1}$  peak after the addition of water.

### 3.4. EXAFS studies

All  $\beta_{\text{bc}}\text{-Ni}(\text{OH})_2$  specimens were investigated; a sixth specimen, a well-crystallised  $\beta\text{-Ni}(\text{OH})_2$ , synthesised following Merlin's method [17] and called 'M hydroxide', was used as a reference.

Fourier-transform infrared spectroscopy pictures of  $\chi(k) * k^2$  are depicted in Fig. 10. This figure shows that the first peak area, which is related to the nearest neighbour Ni-O, and that of the second peak relative to Ni-Ni bonding decrease from hydroxide E to hydroxide A. The spectra relative to the other  $\beta_{\text{bc}}\text{-Ni}(\text{OH})_2$  samples are not given, but the surface areas of their peaks change progressively: they decrease with decreasing crystallinity. This could be interpreted as the expression of the existence of  $\text{OH}^-$  vacancies.

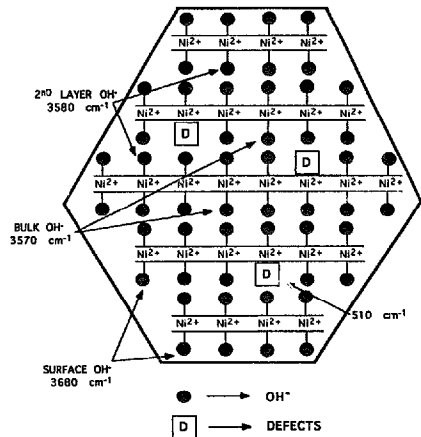


Fig. 9. Illustration of the origin of the three additional Raman peaks.

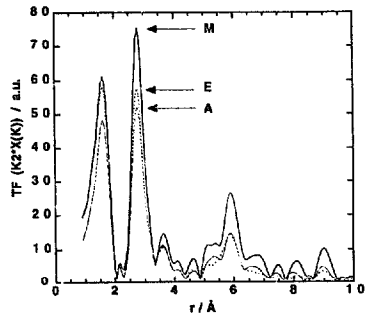


Fig. 10. Fourier-transform magnitude spectra (uncorrected for phase shift) of the hydroxides M, E and A.

These vacancies may compensate for the excess of negative charges induced by proton vacancies pointed out above. One may consider that this excess of negative charges will be neutralised by an increase of the oxidation state of nickel atoms. However, Fig. 11 indicates that the threshold energy is the same for all hydroxides, this hypothesis should be therefore rejected. The  $\text{OH}^-$  vacancies would then compensate for the excess of negative charges due to the presence of  $\text{O}^{2-}$  atoms, the latter induced by proton vacancies. The  $\text{OH}^-$  vacancies could be present at the surface of the crystallites, but it is difficult to imagine these vacancies in the bulk because of the great size of the empty space they would generate. Nevertheless, XRD and Raman spectroscopy experiments suggest strongly the presence of proton vacancies in the bulk of the crystallites. These results imply that they must be compensated in the bulk. The bulk defects could be proton

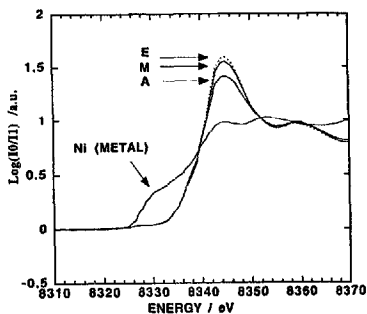


Fig. 11. Absorption spectra of the hydroxides M, E and A.

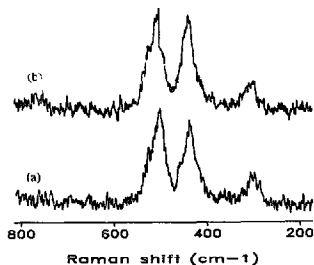
vacancies associated with  $H_2O$  molecules which existence in  $\beta_{Ni}-Ni(OH)_2$  has already been demonstrated [18,19]. Furthermore, proton vacancies may explain why the proton diffusion coefficient is greater when the crystallinity of  $\beta_{Ni}-Ni(OH)_2$  is lower, as illustrated very recently by Watanabe et al. [8].

### 3.5. Effect of co-precipitated additives

The effect of co-precipitated additives usually associated with nickel in nickel hydroxide, such as cadmium and cobalt, has been studied, in particular, their influence on the rate of defects, i.e. proton vacancies.

#### 3.5.1. Effect of co-precipitated cadmium

The incorporation of cadmium into the  $\beta_{Ni}-Ni(OH)_2$  structure does not modify the Raman spectra presented in Fig. 12. It has only slightly modified the  $a$  and  $c$  lattice parameters, because the cadmium ion is greater than the nickel ion, as illustrated in Table 4. In general, the addition of any foreign ion at an oxidation level (+II) inside the nickel hydroxide crystal should not modify the amount of proton vacancies.

Fig. 12. Effect of the ratio of co-precipitated cadmium on the Raman spectra of  $\beta_{Ni}-Ni(OH)_2$ : (a)  $\beta_{Ni}Ni_{0.95}Cd_{0.05}Co_{0.01}(OH)_2$ , and (b)  $\beta_{Ni}Ni_{0.92}Cd_{0.07}Co_{0.01}(OH)_2$ .Table 4  
Ionic radius of Ni, Co and Cd

Element	Ni <sup>2+</sup>	Co <sup>3+</sup>	Cd <sup>2+</sup>
Ionic radius (Å)	0.72	0.63	0.97

#### 3.5.2. Effect of co-precipitated cobalt

The incorporation of cobalt in  $\beta_{Ni}-Ni(OH)_2$  leads to an increase of the relative intensity of the  $510\text{ cm}^{-1}$  Raman peak, Fig. 13. Its relative surface (compared with that of the  $460\text{ cm}^{-1}$ ) is a linear function of the co-precipitated cobalt ratio, Fig. 14. This suggests that the presence of co-precipitated cobalt increases the number of proton vacancies, e.g. the fact that cobalt is not co-precipitated as  $Co^{2+}$  cations but as  $Co^{3+}$ . Thus, the insertion of one cation in the nickel hydroxide lattice creates one proton vacancy.

The increase of the number of proton vacancies seems to be confirmed by the observation of the evolution of the  $a$  and  $c$  lattice parameters. In particular, the  $c$  value decreases when the cobalt ratio increases, see Table 5. Such a relationship between the decrease of the  $c$  value and the increase of the intensity of the  $510\text{ cm}^{-1}$  Raman peak was already observed with  $\beta_{Ni}-Ni(OH)_2$  containing no co-precipitated additives.

The  $\beta_{Ni}-Ni(OH)_2$  hydroxides containing different rates of co-precipitated cobalt were selected to present a crystallite size

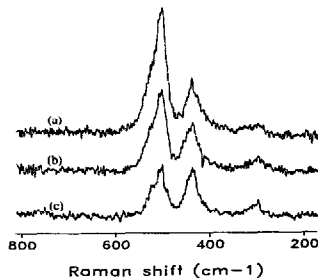
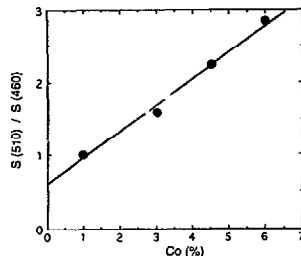
Fig. 13. Effect of the ratio of co-precipitated cobalt on the Raman spectra of  $\beta_{Ni}-Ni(OH)_2$ : (a)  $\beta_{Ni}Ni_{0.97}Cd_{0.07}Co_{0.06}(OH)_2$ ; (b)  $\beta_{Ni}Ni_{0.94}Cd_{0.07}Co_{0.01}(OH)_2$ , and (c)  $\beta_{Ni}Ni_{0.92}Cd_{0.07}Co_{0.01}(OH)_2$ .Fig. 14. Surface of the  $510\text{ cm}^{-1}$  Raman peak (relative to that of the  $460\text{ cm}^{-1}$  peak) as a function of the ratio of co-precipitated cobalt.

Table 5  
Crystallographic parameters of different  $\beta_{bc}\text{-Ni}_{0.91-x}\text{-Co}_x\text{Cd}_{0.07}(\text{OH})_2$

Hydroxide	$\text{Ni}_{0.915}\text{Co}_{0.015}\text{Cd}_{0.07}(\text{OH})_2$	$\text{Ni}_{0.91}\text{Co}_{0.02}\text{Cd}_{0.07}(\text{OH})_2$	$\text{Ni}_{0.89}\text{Co}_{0.03}\text{Cd}_{0.07}(\text{OH})_2$	$\text{Ni}_{0.89}\text{Co}_{0.04}\text{Cd}_{0.07}(\text{OH})_2$
$a$ (Å)	3.124	3.123	3.123	3.123
$c$ (Å)	4.631	4.642	4.645	4.658
Crystallite size (Å)	55	51	57	59

identical to that of compound A (which offers the best reactivity). Their Raman spectrum in the 4000–2000  $\text{cm}^{-1}$  zone were for all of them identical to that of compound A.

Those observations lead to the following remarks:

(i) these data re-inforce the hypothesis: the relative intensity of both 3680 and 3580  $\text{cm}^{-1}$  Raman peaks (compared with that of the 3570  $\text{cm}^{-1}$  one) are associated with the surface area of the crystallites, and

(ii) the crystallite size and the proton vacancies ratio are not merely linked based on the behaviour of different  $\beta_{bc}\text{-Ni}(\text{OH})_2$  compounds containing no co-precipitated additives (compounds A to E).

Finally, the addition of any foreign ion at an oxidation level (+III) inside the nickel hydroxide crystal should increase the amount of proton vacancies.

#### 4. Conclusions

XRD and Raman spectroscopy can be used as simple techniques to predict the electrochemical reactivity of  $\beta_{bc}\text{-Ni}(\text{OH})_2$ . With these methods excessive cell measurement can be avoided in order to compare electrochemical discharge data of some  $\text{Ni}(\text{OH})_2$  samples at well-defined conditions of the preparation of electrodes.

Moreover, these techniques give interesting information on the understanding of the parameters governing the electrochemical efficiency of  $\beta_{bc}$ -nickel hydroxide. This latter seems to be linked not only with the crystallite size [6–9] but also with the existence of proton vacancies:

(i) the crystallite size can be estimated from the width of XRD peaks, and from the relative surface of both the 3680 and 3580  $\text{cm}^{-1}$  Raman peaks, and

(ii) the amount of proton vacancies can be estimated by measuring the relative surface of the 510  $\text{cm}^{-1}$  Raman peak.

For a given chemical composition of  $\beta_{bc}\text{-Ni}(\text{OH})_2$ , the number of proton vacancies increases when the crystallite size decreases. However, the addition of co-precipitated cobalt gives rise to an important increase in proton vacancies, irrespective of the crystallite size of the material.

Finally, it is shown that proton vacancies shifts the oxidation potential of  $\text{Ni}(\text{OH})_2$  towards more cathodic values. This phenomena should improve the chargeability and the charge retention of the positive nickel hydroxide electrode.

#### Acknowledgements

The authors wish to thank the ANRT for its financial support, and Dr Fillaux, Professor Lecerf and Professor Delmas for their helpful discussions.

#### References

- [1] M. Oshitani, H. Yufu, K. Takashima, S. Tsuji and Y. Matsumaru, *J. Electrochem. Soc.*, **136** (1989) 1590.
- [2] M. Watada, M. Ohnichi, Y. Harada and M. Oshitani, *Yuasa-Jiho*, **70** (1990) 4.
- [3] Matsushita, *JP Patent No. 7793* (19 Jan. 83).
- [4] J. Babjak, V.A. Eitel, M.A. Mosouh and P. Kalal, *Ext. Abstr., The Electrochemical Society, Fall Meeting, New Orleans, LA, USA, 1993*, Proc. Vol. 2, 1993, p. 100.
- [5] C. Audry, P. Bernard, A. Lecerf and S. Senyariach, *Patent Pend. No. 9 502 504* (3 Mar. 1995).
- [6] A. Delahaye, *Ph.D. Thesis*, University of Picardie, 1986.
- [7] M. Terasaka, M. Kanbayashi and T. Shoji, *JP Patent No. 541 213* (6 Aug. 1991).
- [8] K. Watanabe, T. Kikuoka and N. Kumagai, *J. Appl. Electrochem.*, **25** (1995) 219.
- [9] R. Bernard, C.F. Randall and F.L. Tye, in J. Thompson (ed.), *Power Sources 8*, Academic Press, London, 1981, pp. 401–423.
- [10] P. Scherrer, *Gött. Nachr.*, **2** (1918) 98.
- [11] C. Johnston and P.R. Graves, *Appl. Spectrosc.*, **44** (1990) 105.
- [12] F.P. Kober, *J. Electrochem. Soc.*, **114** (1967) 215.
- [13] B.C. Cornilisen, P.J. Karjala and P.L. Loyselle, *J. Power Sources*, **22** (1988) 351.
- [14] C. Faure, C. Delmas and M. Fouassier, *J. Power Sources*, **35** (1991) 279.
- [15] A. De Roy, J.P. Besse and P. Bondot, *J. Phys. (Paris)*, **47** (1986) C8-713.
- [16] C. Greaves and M.A. Thomas, *Acta Crystallogr.*, **B42** (1986) 51.
- [17] A. Merlin and S.J. Teicher, *C.R. Acad. Sci.*, **236** (1953) 1892.
- [18] M. Figlarz and S. Le Bihan, *C.R. Acad. Sci., Ser. C*, **272** (1971) 580.
- [19] M.J. Avena, M.V. Vazquez, R.E. Carbonio, C.P. De Pauli and V.A. Macagno, *J. Appl. Electrochem.*, **24** (1994) 256.